

The role of collective pitch in multi rotor UAV aerodynamics

D. Langkamp, W.J. Crowther

University of Manchester

George Begg Building, Sackville Street, Manchester, M13 9PL, david.langkamp@postgrad.manchester.ac.uk

Abstract

Small multi rotor UAVs, such as quadrotors, are increasingly being considered for operations in urban environments. Two key problems with current fixed-pitch, variable speed rotor vehicles are their endurance and ability to fly under gusty conditions. The aim of the work in this paper is to explore the effects of introducing a variable pitch capability on propulsive efficiency and open-loop response to velocity disturbances. The simulation method is based on a numerical blade element code combined with a range of 1st order inflow models. Extensive wind tunnel testing of a small-scale variable pitch rotor system was carried out to provide validation cases. Results show that moderate collective pitch angles can enhance vehicle endurance compared to lower and higher collective pitch settings, whilst large collective pitch angles can significantly improve the initial vehicle gust response.

Introduction

Small multi rotor UAVs are currently being widely considered for civil and military operations in urban environments [1]. These vehicles are typically electrically powered and have low disk loadings to achieve operationally useful flight duration. Low disk loading does however create problems under gusty conditions, leading to limited all weather capability for these systems. Quadrotor-type vehicles are typically controlled by varying the rotational speed of individual fixed-pitch rotors, and are widely used as an alternative to conventional helicopter designs for UAV in the range of a few kg where mechanical simplicity is more important than manoeuvrability or duration.

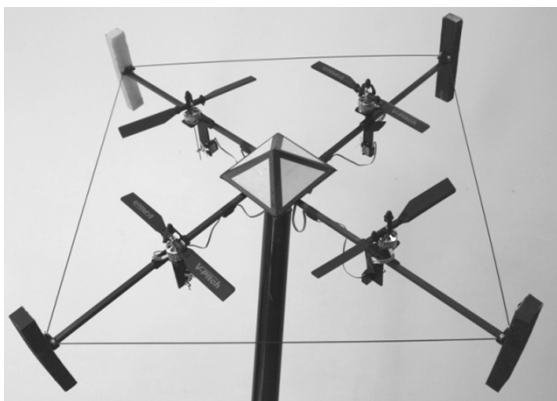


Figure 1: Variable pitch quadrotor prototype on teststand. Take-off mass 0.75kg, rotor radius 0.127m

This paper considers the rotor design for variable pitch quadrotors for which flight control inputs are provided by variation in rotor collective pitch and/or

change in rotor speed. An image of a prototype vehicle developed for the present work is shown in Figure 1. One of the key differences is that for the variable pitch vehicle the required thrust level can be achieved using a combination of collective pitch and rotational speed. This promises both enhanced manoeuvrability compared to fixed-pitch designs and the ability to tailor rotor aerodynamic properties to the flight condition at the cost of increased mechanical complexity. It could also allow the design of larger quadrotors, where scaling effects prevent the design of larger variable-speed quadrotors due to the increased control response time associated with larger rotor diameters and inertia.

Small rotary wing vehicles typically operate at Reynolds numbers several orders of magnitude smaller than large scale helicopters. As such one of their key problems is lower efficiency [2] and hence endurance. The second key problem of any small UAV design is the ability to fly in the turbulent urban environment [3].

Quadrotor UAVs have been subject of numerous scientific papers in the recent years. Most papers on this topic have a clear focus on control and autonomy issues (such as [4]) and virtually all published work focus on fixed-pitch variable speed quadcopters.

The few publications dealing with quadrotor aerodynamics (such as [5],[6], [7]) are predominantly based on the use of basic aerodynamic models such as actuator disk theory [6] or analytical solutions to the blade element theory [7]. More recent work [5] is

considering the effects of forward flight and the effect of gusts on quadrotors [8].

These models do not fully capture the effects of the blade geometry, the influence of the vehicle velocity vector or the nonlinear aerodynamics. Including these effects is, however, necessary to explore the effects a variable pitch capability could have on endurance and thrust variation with the free stream velocity vector. Furthermore experimental rotor force data of relevant Reynolds number and velocity vectors is very limited.

In this paper a comprehensive numerical blade element code is presented which combines nonlinear aerodynamic and blade geometry models with 1st order inflow models for forward flight and vortex ring state cases.

Hover and wind tunnel testing results for a small scale variable pitch rotor of 0.127m rotor radius are presented. Finally the implications of the results are discussed with respect to the influence of rpm/collective pitch demands on rotor power and thrust variation with airspeed.

The work presented in this paper for the first time shows how collective pitch could be used to favourably tailor the variation of rotor forces with airspeed.

Method

Performance metrics

Two primary performance metrics were selected to compare the effect of different rotor speed/pitch: First the required rotor power/thrust ratio as an indicator of endurance and second the relative change in rotor force coefficients from hover conditions due to changes in free stream wind vector as an indicator of the initial open-loop vehicle response.

Assumptions and Limitations

Some assumptions in the modelling process are unique to electrical powered vehicles. A variable pitch quadrotor has two control demands: Collective pitch and the rotor speed. The rotor speed is governed by an electronic speed controller. Rotor speed and collective pitch stay constant unless changed by the control loops and hence simplifying assumptions such as level flight or constant power cannot be used to evaluate the initial open-loop thrust response to changes in the free stream velocity vector onto the rotor disk.

One key assumption in the current method is the use of quasi steady aerodynamics. This is justified by the relatively short time constant of the dynamic inflow

for the class of vehicle concerned. The time constant of the dynamic inflow ODE [2] is

$$\tau_\lambda = \frac{0.849}{4\bar{\lambda}_t\Omega}$$

For quadrotors of a few kg mass the typical rotational speeds ($\Omega = 450$ rad/s) and a mean hover inflow ratio ($\bar{\lambda}_t = 0.08$) this yields a time constant of 6 ms, which is an order of magnitude smaller than on typical full scale helicopters.

The current paper is solely based on the open-loop aerodynamic effects on the rotor and hence motor performance and control laws are not included. Another limitation is that rotors are treated as independent. Parts of the following methodology were presented in [9] and are included here for completeness.

Wind Tunnel testing

Apparatus

A commercial off the shelf variable pitch system as typically found on fixed wing ‘shock’ flyer model aircraft was used as the test article. The system was driven by a brushless motor controlled by an off the shelf electronic speed controller [ESC]. The collective pitch mechanism was based on a simple pitch linkage rod through a hole in the rotorshaft, thus avoiding the need for a swashplate. The mechanism was driven by a digital servo.

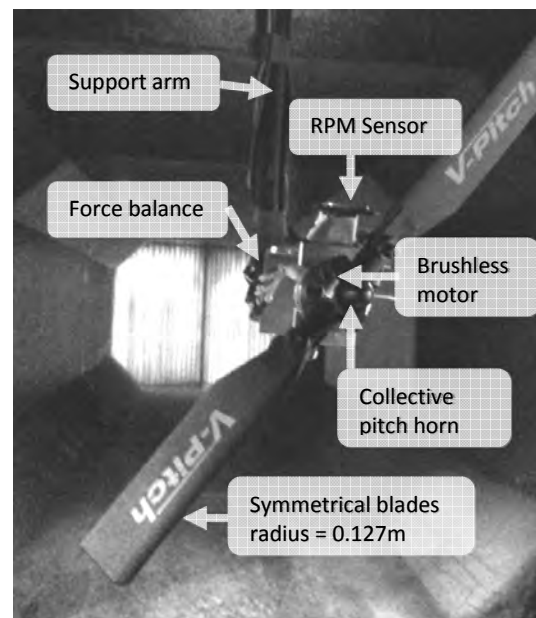


Figure 2: Variable pitch wind tunnel test rig with force balance and rpm sensor. Rotor diameter = 254 mm.

The rotor radius was 0.127 m and the solidity was 0.099. The blades were symmetrical and untwisted with a constant chord between 40-100% radius. The Reynolds number at $\frac{3}{4}$ radius varied between 20 000

– 130 000. The thickness to chord ratio was measured as 12%.

The rotor was tested in an open-circuit blow down low speed tunnel with a 0.9x11.m test section and a turbulence level of 0.5% [10]. A 6-axis force balance was fitted between the motor and the support arm. Motor bracket and strut were designed to minimise the blockage directly behind the rotor whilst allowing for a 360° rotation using the overhead yaw control mechanism. The assembly was equipped with a Hall effect sensor for the rotational speed and pressure transducers for the tunnel velocity.

Real-time data acquisition equipment was used to take simultaneous measurements of all sensors and set demands for collective pitch and rpm.

Procedure

Pressure transducers and force balance were calibrated. Ambient pressure and temperature readings were taken before and whilst conducting the experiments. The pitch angle of the non-rotating rotor was measured manually and calibrated against position demand of the digital servo.

Sensitivity studies were carried out under hover conditions to optimise settling time and sampling rates of the data acquisition equipment and ensure repeatability of the results.

To avoid excessive interference of the rotor on the test section velocity measurements, the test section velocity was determined by relating measurements of the pressure in the settling chamber ahead of the contracting cone with the static pressure before the test section. This is standard wind tunnel practice as presented in [11].

Test parameters were tunnel speed, rotor disk incidence α_{disk} , rotor speed and collective pitch angle. The measured variables were 6 components of force/moment, rotor speed, tunnel velocity and motor absorbed electrical power. At every tunnel setting a sequence of rotational speed and collective pitch combinations was repeated to map out the changes in rotor force coefficients up to a horizontal (tangential to disk) advance ratio of 0.2 and for vertical (perpendicular) advance ratios from -0.2 to 0.2. The same collective pitch/rotor speed sequences were repeated under static hover conditions to provide a benchmark case. In total about 6000 different advance ratio/pitch combinations were measured.

Data reduction

The tunnel velocity and disk angle were resolved into tangential and perpendicular components to the disk and then nondimensionalized against the rotor tip

speed to give the horizontal (forward flight) and vertical (climb/descent) advance ratios:

$$\mu_x = \frac{V_x}{\Omega R}; \quad \mu_z = \frac{V_z}{\Omega R};$$

All forces were expressed in coefficient form by nondimensionalizing with disk area, density and the square of the tip speed:

$$C_T = \frac{T}{\rho A (\Omega R)^2} \quad C_Q = \frac{Q}{\rho A R (\Omega R)^2} \quad C_P = \frac{P}{\rho A (\Omega R)^3}$$

Thrust and power were further expressed as a ratio of the hover value to clarify the relative response of a trimmed system to non-stationary flight conditions.

Corrections and Uncertainty analysis

To evaluate the tunnel interaction effects a boundary correction calculation according to Glauert [12] was carried out:

$$\frac{V'}{V} = \left(1 - \frac{\tau_4 \alpha_1}{2\sqrt{1+2\tau_4}} \right)$$

$$\text{with } \tau_4 = \frac{T}{\rho A_{disk} V^2}; \quad \alpha_1 = \frac{A_{disk}}{A_{tunnel}}$$

It was found that for typical test conditions ($T = 2N$, $V < 10m/s$) the velocity correction is $< 3\%$ and could be neglected.

An uncertainty analysis was carried out considering the effect of sensor uncertainty on the uncertainty on thrust and torque coefficients. Experimental uncertainty was highest at low thrust settings due to the finite resolution of the force balance. Thrust settings at around 50% of hover resulted in uncertainty of around 5% at a 95% confidence interval, and thrust level below this threshold are generally not included in the results dataset.

Blade Element Simulation

A numerical blade element code was written to provide an estimate of forces, moments and power for a given rpm/pitch demand. The code does not require a priori knowledge of blade loading. It can be used to gain an insight into what is happening at the rotor blade level in forward flight, like the angle of attack distribution on the blade. The user inputs are rotor geometry, airfoil data, rotor angular speed, rotor collective pitch and the free stream velocity vector.

The code uses two iteration loops: An outer loop for the blade loading and an inner iteration loop to match the inflow conditions to the current loading conditions.

Blade Element modelling approach

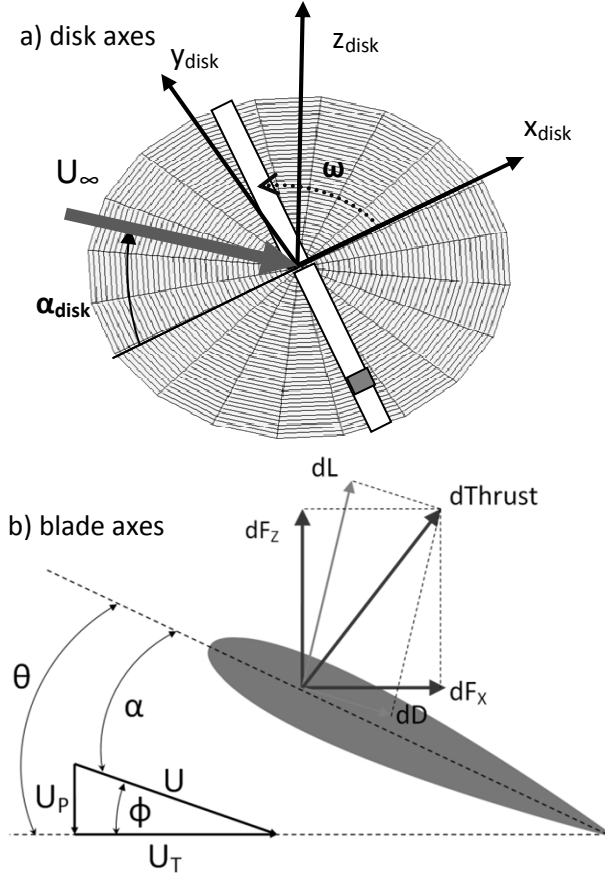


Figure 3: Disk and local blade element coordinate systems

First the blade is broken down into M radial elements and the swept disk into K azimuthal stations. Every blade element is treated as an independent 2-D airfoil section. The flow is modelled as incompressible, justified by the low (<0.25) tip Mach numbers typical for the class of rotary wing vehicles considered.

The velocity at every blade element in forward flight conditions is decomposed into a tangential, perpendicular, and radial component, respectively:

$$U_t(y, \psi) = \Omega y + U_\infty \sin \psi$$

$$U_p(y, \psi) = V_c + v_i + y\dot{\beta}(\psi) + U_\infty \beta(\psi) \cos \psi$$

$$U_r(\psi) = U_\infty \cos \psi$$

The angle β represents the periodic flapping angle, which is induced by the asymmetry of lift in forward flight. The radial components can be neglected for the lift estimation [2] and the resultant velocity on the blade element is now:

$$U = \sqrt{U_T^2 + U_P^2}$$

As shown in Figure 3 the velocity components can be used to calculate the inflow angle and the local angle of attack, respectively, as:

$$\phi = \tan^{-1} \left(\frac{U_P}{U_T} \right) \quad \alpha = \theta - \phi$$

The lift and drag per blade element can be expressed as:

$$dL = \frac{1}{2} \rho U^2 c C_L(\alpha, Re, r) dy$$

$$dD = \frac{1}{2} \rho U^2 c C_D(\alpha, Re, r) dy$$

Finally, the forces acting on the blade element are resolved in disk axes via

$$df_z = dL \cos \phi - dD \sin \phi$$

$$df_x = dL \sin \phi + dD \cos \phi$$

The force components are then integrated along the blade radius and averaged for the azimuthal stations over one rotation to obtain the overall 6-DoF forces and moments produced by the rotor.

Airfoil Characteristics

Most analytical solutions in the literature are based on linear aerodynamic models using a constant lift curve slope. These models are unable to capture the non-linearities of lift and drag at higher blade element angles of attack. In the present work, a 2-D lookup-table was used to obtain C_L and C_D as a function of Reynolds number and angle of attack. A $\pm 180^\circ$ angle of attack range was used to represent the full range of possible flow conditions, including reversed flow. The lookup table was populated with simulation results from Xfoil and limited experimental data [13] for similar Reynolds numbers. Considering the limited availability of reliable experimental data for the relevant Reynolds numbers, the airfoil model is subject to considerable uncertainty.

Induced Velocity Modelling

A key challenge in applying the blade element method is appropriate modelling of the induced velocity. Whilst Blade Element Momentum theory solutions for hover, climb and uniform inflow are well documented, further modelling is needed to obtain a realistic distribution of induced velocity across the disk for all flight conditions. The challenge lies in combining existing models for forward flight and descent to provide a continuous and representative simulation.

Glauert's solution [2] for forward flight cases uses the conservation laws to relate thrust, mass flow and uniform induced velocity as

$$T = 2\dot{m}v_i$$

In order to give a radial distribution of the induced velocity in forward flight and climb, this equation was re-written based on small radial annuli:

$$dT = 2\dot{m}_{annulus}v_i(r) = 2(\rho A_{annulus}U_{annulus})v_i(r)$$

$$dT = 2\rho A_{annulus}v_i(r)\sqrt{V_x^2 + (V_z + v_i(r))^2}$$

With the area of annulus being

$$A_{annulus} = 2\pi y dy$$

The local inflow induced velocity was then expressed as a function of the local element loading

$$v_i(r) = \frac{dT}{4\pi y dy \sqrt{V_x^2 + (V_z + v_i(r))^2}}$$

and solved by a Newton-Raphson iteration scheme with a convergence criterion of a 0.005% error in $v_i(r)$.

The new radial inflow distribution is being fed back into the numerical blade element code to provide a revised estimate of the blade loading – hence an outer iteration loop is required until the blade loading distribution converges.

The proposed method is valid for hover and climb cases and numerically stable for forward flight with a slight descent angle.

For the special case of axial descent in the vortex ring state a semi-empirical solution from literature was used to approximate the uniform induced velocity in the entire vortex-ring state [2]:

$$\frac{\lambda_i}{\lambda_h} = k + k_1\left(\frac{V_c}{v_h}\right) + k_2\left(\frac{V_c}{v_h}\right)^2 + k_3\left(\frac{V_c}{v_h}\right)^3 + k_4\left(\frac{V_c}{v_h}\right)^4$$

Where k is the measured induced power factor in hover and Leishman suggests the coefficients as: $k_1 = -1.125$, $k_2 = -1.372$, $k_3 = -1.718$, $k_4 = -0.655$.

Key limitations of using this vortex ring state model are that it can only give a uniform inflow, hence introducing a discontinuity in the rotor force model when it is switched between axial climb and descent, and that it does not make any provision for effects from forward flight.

Tip loss model

The tip losses were modelled by including Prandtl's tip loss function [2]

$$F = \frac{2}{\pi} \cos^{-1} \exp((-f)) \quad \text{with } f = \frac{N_b}{2} \left(\frac{1-r}{r \sin \phi} \right)$$

into the induced velocity iterations. This increases the inflow towards the blade tips and decreases the blade loading as shown in Figure 9.

First harmonic inflow models for forward flight

In forward flight the induced velocity field is no longer axisymmetric and the wake is inclined by a wake skew angle X , which is dependent on the velocity vector on the rotor disk:

$$X = \tan^{-1} \left(\frac{\mu_x}{\mu_z + \bar{\lambda}_i} \right)$$

The wake skew angle forms the basis for most first harmonic inflow models which express the lateral and longitudinal variations of the induced velocity along the rotor disk by the coefficients K_x and K_y and the average induced velocity from momentum theory λ_0 :

$$\lambda_i = \lambda_0 \left(1 + \frac{x}{R} k_x + \frac{y}{R} k_y \right)$$

A range of inflow models reviewed by Chen [14] were implemented in the blade element code. The best agreement with the wind tunnel results was obtained with the models by Pitt/Peters and Drees. Inflow results of the Drees model coupled with the radial inflow solution are shown in Figure 4.

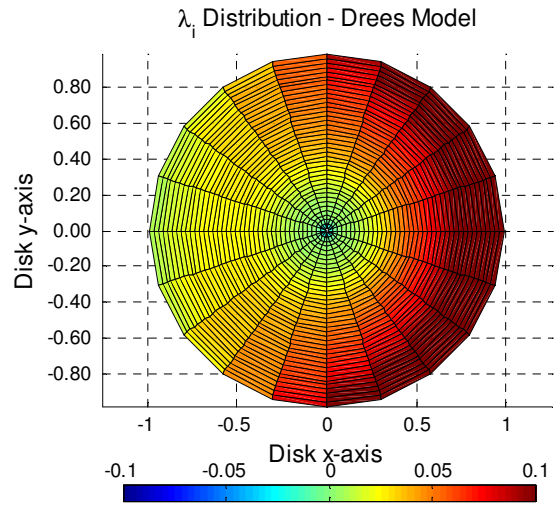


Figure 4: Inflow distribution in forward flight at $\mu=0.2$ showing a clear bias towards the rear of the disk

Blade Element Model validation

Figure 5 compares the simulated hover thrust and power coefficients with experimental data. The power coefficient data, Figure 5b), data shows a good agreement at lower collective pitch angles, however there is a clear deviation in correlation from around 15° pitch, consistent with where the thrust coefficient, figure 5a), departs from the linear trend.

This region beyond a blade pitch angle of 15° is most influenced by the uncertainty in the nonlinear lift model.

In forward flight and climb the experimental thrust trend (not shown) is captured well by the model, however the model deviates significantly for steep descent.

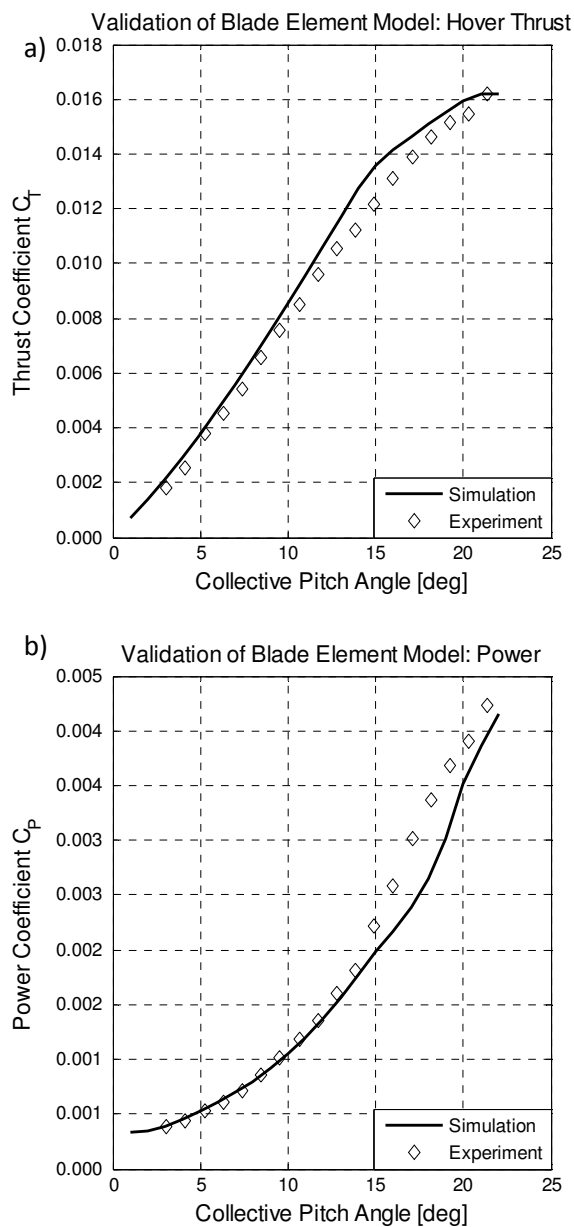


Figure 5: The blade element results are showing a good agreement with experimental thrust and power coefficients

Results

Effect of Collective Pitch on Power

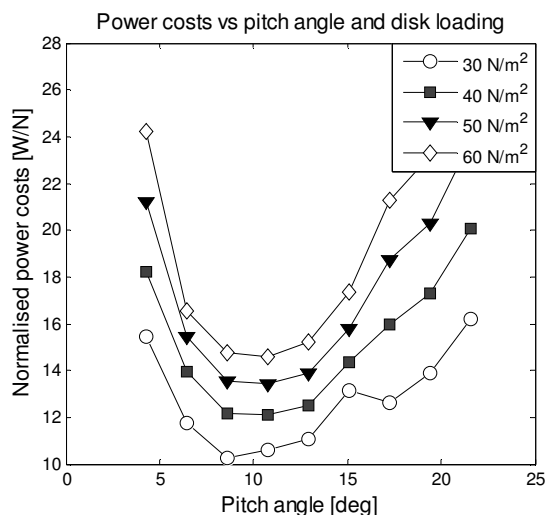


Figure 6: The effect of pitch angle and disk loading on thrust specific power.

Figure 6 shows the relative power costs per Newton of hover thrust for a range of practical quadrotor disk loadings. As expected from theory, an increase in disk loading increases the power costs and hence decreases efficiency. The u-shaped profile indicates that there is optimum pitch angle for minimum power costs.

Effect of Collective Pitch on Thrust response

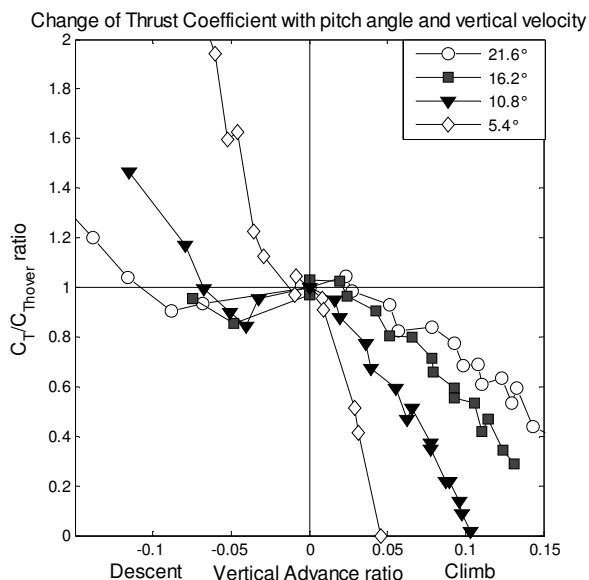


Figure 7: Impact of collective pitch on thrust coefficient ratio in vertical flight

Figure 7 shows the effect of the collective pitch angle on the thrust coefficient ratio change with climb and descent. It can be clearly seen that an increase in collective pitch significantly reduces the variation of the rotor thrust coefficient with the vertical advance ratio. The only exception to this is the data in the

vortex ring state regime in slow descent, which is inconclusive.

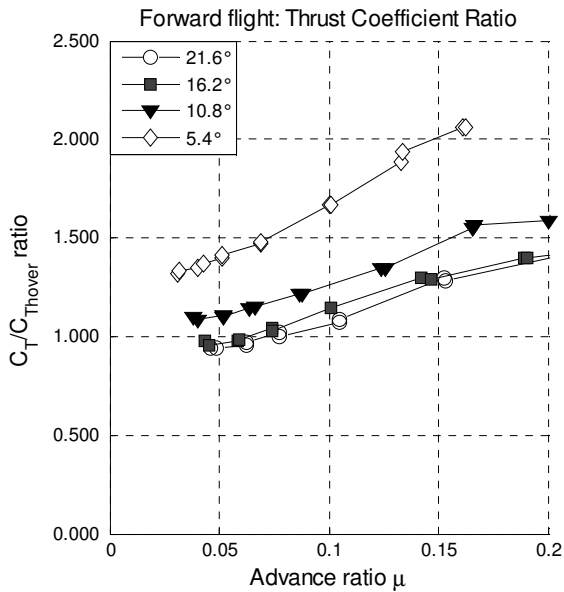


Figure 8: Thrust coefficient ratio in forward flight

The effect of high collective pitch for a rotor in forward flight is shown in Figure 8. Whilst significant benefits can be achieved by moving from 10.8° to 16.2°, a further increase in collective pitch brings only minimal benefits.

Inensitivity of spawise loading

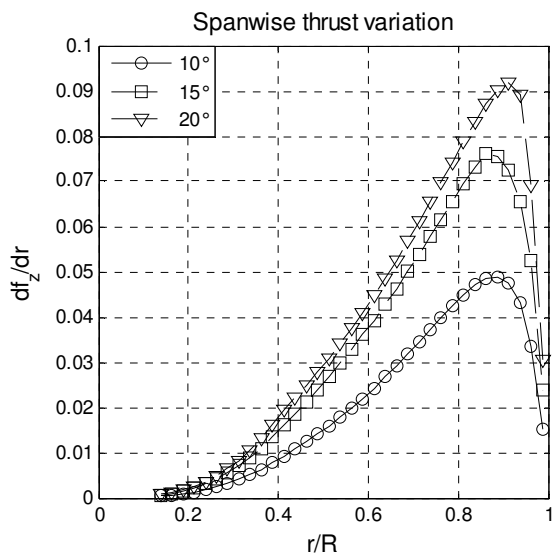


Figure 9: The spanwise thrust variation becomes less sensitive to further pitch changes

Figure 9 shows the blade element results of the nondimensional spanwise blade loading for different collective pitch settings. It can be seen that the loading at higher pitch angles gets less sensitive to further changes. Simulation results suggest that a similar effect is driving the velocity insensitivity at high collective pitch angles, where large areas of the

rotor disk are moved in the non-linear region of the lift curve where the slope is reduced. Hence a change in local angle of attack induced by changes in the free stream velocity has a less strong effect on the local lift. This makes the thrust coefficient less sensitive to velocity variations at the expense of decreased efficiency.

Implications of the results

Since the comparison was done on the basis of thrust coefficients and constant rpm/collective pitch demands the ratio gives an indication of the initial open-loop vehicle response. The significance of the observed effect is that it could be exploited to reduce the initial response of rotary-wing vehicles to velocity disturbances.

Rather than using collective pitch only as control input it could be also used for in combination with variable-speed control to favourably tailor the rotor force landscape. One option could be switching between more efficient medium pitch settings and high pitch settings. This change could be performed during a mission and could expand the operational envelope to higher velocities and improved gust response compared to fixed-pitch quadcopter rotors without increasing the overall disk loading.

As shown in the results there is limited additional benefit of increasing collective pitch beyond a certain point, whilst collective pitch angles beyond the optimum efficiency region will decrease efficiency. A careful trade-off between both effects allows the selection of a collective pitch setting which desensitises the thrust response to velocity changes for an acceptable increase in power demand.

Conclusions

Experimental data from a small scale ($R= 0.127\text{m}$) variable pitch rotor system has shown that variable collective pitch can be used to desensitise the velocity disturbance response of rotorcraft vehicles, such as quadrotors, at the expense of increased power consumption. Together with the proposed methodology this presents a contribution to the field of quadrotor aerodynamics which could lead to improved vehicle performance in non-stationary flight and turbulent environments.

Next steps will include further research into the optimum trade-off for collective pitch settings and the flight testing of a variable pitch quadcopter UAV (shown in Figure 1).

Acknowledgements

The authors would like to thank Phil Geoghegan, Matt Pilmoor, Ian Lunnon and Andrew Kennaugh for their support with the experimental setup.

References

1. Samad, T., *Network-centric systems for military operations in urban terrain: the role of UAVs*. Proceedings of the IEEE, 2007. **95**(1): p. 92.
2. Leishman, J.G., *Principles of Helicopter Aerodynamics 2nd edition*. 2006, Cambridge: Cambridge Aerospace Series.
3. *Capability Challenges Document*. January 2010, SEAS DTC.
4. Bouabdallah, S., P. Murrieri, and R. Siegwart, *Towards autonomous indoor micro VTOL*. Autonomous Robots, 2005. **18**(2): p. 171-183.
5. Bristeau, P., Martin, P., Salauen, E., Petit, N., *The Role of Propeller Aerodynamics in the Model of a Quadrotor UAV*, in *Proceedings of the European Control Conference 2009*. 2009: Budapest.
6. Hoffmann, G.M., Huang, H., Waslander, S.L., Tomlin, C.J., *Quadrotor Helicopter Flight Dynamics and Control: Theory and Experiment*, in *AIAA Guidance, Navigation and Control Conference and Exhibit, 20-23 August 2007*. 2007, AIAA: Hilton Head, South Carolina.
7. Valavanis, K.P., *Advances in Unmanned Aerial Vehicles: State of the Art and the Road to Autonomy*. 2007: Springer.
8. Waslander, S., Wang, C., *Wind Disturbance Estimation and Rejection for Quadrotor Position Control*, in *Infotech @ Aerospace Conference 2009, AIAA Unmanned Unlimited Conference*. 2009: Seattle, Washington.
9. Langkamp, D., Crowther W.J., *A low order rotor aerodynamics model for UAVs in wind*, in *2010 RAeS Aerodynamics Conference - Applied Aerodynamics: Capabilities and Future Requirements*. 2010, RAeS: Bristol.
10. Potts, J., *Disc-Wing Aerodynamics*, in *School of Mechanical and Aerospace Engineering*. 2005, University of Manchester: Manchester.
11. Barlow, J.B., Rae, W.H., Pope, A., *Low speed wind tunnel testing - 3rd edition*. 1999, New York: Wiley-Interscience.
12. Glauert, H., *The elements of aerofoil and airscrew theory, 2nd edition*. Cambridge Science Classics. Previous ed. 1926, Cambridge: Cambridge University Press.
13. Bohorquez, F., *Rotor Hover Performance and System Design of an Efficient Coaxial Rotary Wing Micro Air Vehicle*, in *Department of Aerospace Engineering*. 2007, University of Maryland.
14. Chen, R.T.N., *A Survey of Nonuniform Inflow Models for Rotorcraft Flight Dynamics and Control Applications*, in *NASA Technical Memorandum 102219*. 1989, Ames Research Centre.